Int. J. Solids Structures Vol. 28, No. 7, pp. 917–938, 1991
Printed in Great Britain.

0020–7683/91 $3.00 + .00

SAINT-VENANT SOLUTIONS FOR PRISMATIC ANISOTROPIC BEAMS

J. B. KOSMATKA
Department of Applied Mechanics and Engineering Science, University of California, San Diego, La Jolla, CA 92093, U.S.A.

and

S. B. DONG
Department of Civil Engineering, University of California, Los Angeles, CA 90024, U.S.A.

(*Received* 22 *October* 1990; *in revised form* 18 *March* 1991)

Abstract—An analytical model is presented for determining the displacement and stress distributions of the Saint-Venant extension, bending, torsion and flexure problems for a homogeneous prismatic beam of arbitrary section and rectilinear anisotropy. The determination of the complete displacement field requires solving a coupled two-dimensional boundary value problem for the local in-plane deformations and warping out of the section plane. The principle of minimum potential energy is applied to a discretized representation of the cross-section (Ritz method) to calculate solutions to this problem. The behavior of an anisotropic beam is studied in detail using the resulting displacement and stress solutions, where definitions are presented for the shear center, center of twist, torsion constant and a new geometric parameter; the line of extension–bending centers. Two sets of numerical results are presented to illustrate how section geometry, beam length and material properties affect the behavior of a homogeneous anisotropic cantilever beam.

INTRODUCTION

Many current flight structural designs incorporate fiber composite materials as a means of controlling weight, deformation and vibration (i.e. structural tailoring). Although fiber composites are orthotropic at most in material property classification, they can exhibit extension–shear coupling (three-dimensional behavior) when the fiber directions are not oriented parallel or normal to the loads. In beam-type (prismatic) composite structures, such behaviors are commonplace, e.g. Nixon (1987) observed extension–flexure–twist coupling in composite tubes under axial load.

Even though this class of prismatic composite structures is fraught with complicated behavior, one-dimensional beam models have been proposed by Reyfield (1985), Bauchau (1985), Kosmatka (1986) and Kosmatka and Friedmann (1989). The simplifications in these models are derived from assumed kinematic and/or stress fields with the concomitant result that only gross structural responses can be predicted, such as force–moment resultants and bend–twist angles. Two- and three-dimensional stress and displacement fields can be calculated according to the underlying hypotheses (e.g. Bernoulli–Euler and Saint-Venant torsion). However, since transverse shear and normal strains are only approximated as a consequence of these hypotheses, their corresponding stress components are calculated by equilibrium. The veracity and limits of application of these models rest on their comparison with Saint-Venant solutions for extension, bending, torsion and flexure. Saint-Venant solutions also provide data for locating the centroid and shear center as well as calculating the torsion constant, shear correction (shape) factors and other section properties. At present, Saint-Venant analytical solutions are available for homogeneous isotropic beams with simple cross-sections [for example, Sokolnikoff (1946)]. Approximate solutions exist for homogeneous isotropic (Mindlin, 1975; Herrmann, 1965; Mason and Herrmann, 1968) and orthotropic beams (Tolf, 1985), and a restricted class of non-homogeneous, monoclinic beams (Wörndle, 1982). Moreover, while Lekhnitskii's (1963) formulation of this problem for an anisotropic body in terms of Airy and Prandtl stress functions is well known, no solutions are available for a prismatic member with an arbitrary cross-section. In this

respect, Iesan (1976) gave a formal analytical Saint-Venant solution for an inhomogeneous, anisotropic beam, but without results.

Herein, an analytical model is presented for studying Saint-Venant's extension, bending, torsion and flexure problems in a prismatic (beam-type) homogeneous structure of arbitrary cross-section with rectilinear anisotropy. The displacement solutions are based upon Saint-Venant's semi-inverse method, in terms of three applied tip forces, three applied moments, the twist rate and cross-sectional dependent functions defining the local in-plane and out-of-plane deformations inherent in an anisotropic body. The determination of these cross-sectional dependent functions for each of the seven cases (three forces, three moments, twist rate) is accomplished by applying the principle of minimum potential energy, where the cross-section is discretized into quadrilateral and/or triangular subregions with quadratic displacement interpolation (Ritz method). The final form of the displacement and stress field for any combination of the six applied loads involves: first, calculating the cross-section-dependent functions for the appropriate tip loading and for an applied unit twist rate (Saint-Venant torsion), second, the stress fields from these two cases are substituted into the cross-section moment equilibrium equation to determine the actual twist rate that occurs as a result of the applied loading, and finally, the displacement field is written by making use of the calculated twist rate and combining the cross-section-dependent functions via a constraint relation.

Based upon these Saint-Venant solutions, expressions are presented for the shear center, center of twist, torsion constant and for a new geometric parameter called the line of extension–bending centers, where an applied axial force induces bending with no twist. Two sets of numerical results are presented to illustrate how variations in cross-section geometry, beam length and material definition affect the behavior and section properties of an anisotropic cantilever beam. For brevity's sake, many details of the derivation and the validation of the computer code on isotropic beams have been abbreviated or omitted. Readers with further interest are referred to Kosmatka (1986).

It is noted that the Saint-Venant solutions are valid for regions away from the end, i.e. Saint-Venant's principle. Recently, finite element analyses have appeared which address the localized nature of stress and deformation near such boundaries [for example, Giavotto *et al.* (1983); Goetschel and Hu (1985)]. While their finite element discretization procedure is the same as that used herein, these analyses apply to a different set of issues and do not pertain to data for evaluating the usefulness of one-dimensional beam models.

PRELIMINARIES

Consider a cantilevered prismatic beam of length L with an arbitrary cross-section of area A composed of a homogeneous, rectilinearly-anisotropic material. Let rectangular Cartesian coordinates (x, y, z) with corresponding unit vectors (i, j, k) be established with the origin at the centroid of the root end. Orient the (x, y) axes to coincide with the principal axes of the cross-section and let z run parallel to the generator.

Let (u, v, w) denote the displacement components in the coordinate directions and let $\{\sigma\}$ and $\{\varepsilon\}$ denote the arrays of stress and strain whose components are:

$$\{\sigma\}^{\mathrm{T}} = \{\sigma_{xx}, \sigma_{yy}, \sigma_{zz}, \tau_{yz}, \tau_{xz}, \tau_{xy}\},$$
$$\{\varepsilon\}^{\mathrm{T}} = \{\varepsilon_{xx}, \varepsilon_{yy}, \varepsilon_{zz}, \gamma_{yz}, \gamma_{xz}, \gamma_{xy}\}. \tag{1a,b}$$

The strain components are related to the displacements by:

$$\varepsilon_{xx} = \frac{\partial u}{\partial x}, \quad \varepsilon_{yy} = \frac{\partial v}{\partial y}, \quad \varepsilon_{zz} = \frac{\partial w}{\partial z},$$
$$\gamma_{yz} = \frac{\partial v}{\partial z} + \frac{\partial w}{\partial y}, \quad \gamma_{xz} = \frac{\partial u}{\partial z} + \frac{\partial w}{\partial x}, \quad \gamma_{xy} = \frac{\partial u}{\partial y} + \frac{\partial v}{\partial x}. \tag{2a–f}$$

The constitutive relations for a linearly-anisotropic hyperelastic material are given by:

$$\{\sigma\} = [C]\{\varepsilon\},$$
$$\{\varepsilon\} = [S]\{\sigma\},$$
$$[C] = [S]^{-1}, \tag{3a–c}$$

where $[C]$ and $[S]$ are fully-populated symmetric matrices with 21 distinct elements.

The loading and boundary conditions for the problem of coupled extension–bending–torsion–flexure can be stated as follows. The lateral surface is assumed to be traction-free, i.e.

$$\begin{Bmatrix} \sigma_{xx} \\ \tau_{xy} \\ \tau_{xz} \end{Bmatrix} \cos(\hat{n}, x) + \begin{Bmatrix} \tau_{xy} \\ \sigma_{yy} \\ \tau_{yz} \end{Bmatrix} \cos(\hat{n}, y) = \begin{Bmatrix} 0 \\ 0 \\ 0 \end{Bmatrix} \tag{4a–c}$$

where $\hat{n}$ is the unit outward normal. At the root end, the beam is fully fixed. Within the framework of the Saint-Venant problems, this condition cannot be described on a point-wise basis and the equivalent statement at $x = y = z = 0$ can be used:

$$u = v = w = 0,$$
$$\frac{\partial u}{\partial z} = \frac{\partial v}{\partial z} = \frac{\partial v}{\partial x} - \frac{\partial u}{\partial y} = 0. \tag{5a–f}$$

Another acceptable approach for restraining the beam root involves setting to zero the average of the displacements and rotations of the root cross-section [see Mason and Herrmann (1968)].

At the other end, tractions are applied which reduce to an equivalent force P and moment M with respect to the centroid of the cross-section (see Fig. 1). The force P

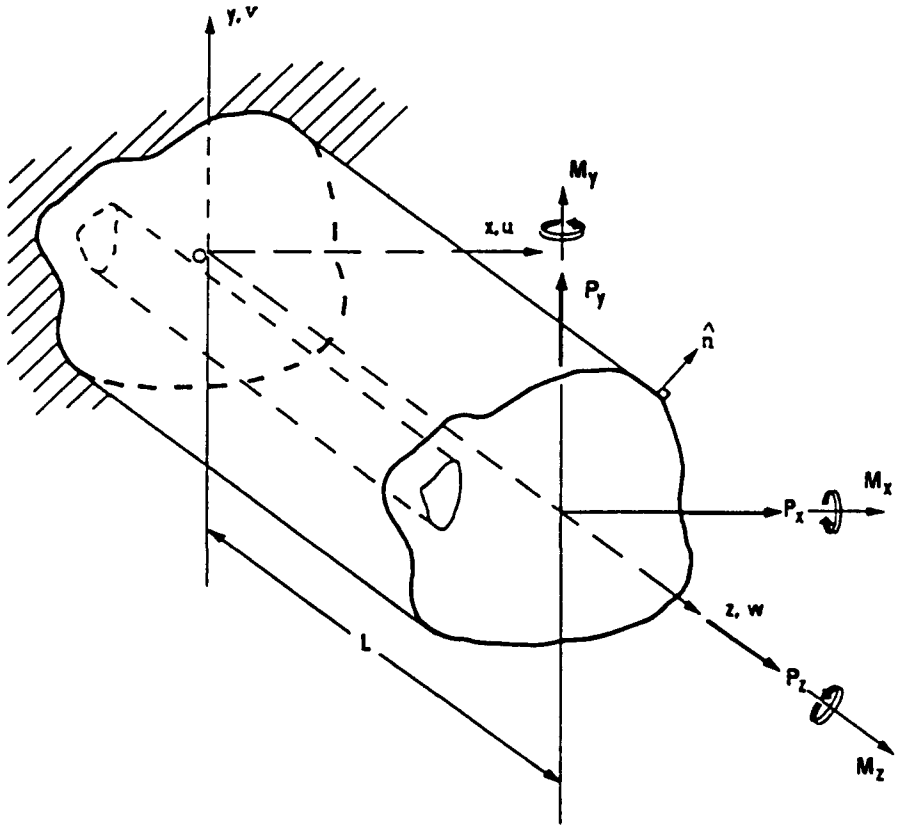

Fig. 1. Anisotropic cantilever beam.

and moment M can be decomposed into flexure components; P_x and P_y, an extensional component; P_z, bending moments; M_x and M_y, and a torsion moment; M_z. The integrals of the tractions over any cross-section ($0 \leqslant z \leqslant L$) yield the following expressions in terms of the six components of force and moment:

$$\int_A \tau_{xz}\,dA = P_x \quad \int_A x\sigma_{zz}\,dA = -M_y - P_x(L-z)$$

$$\int_A \tau_{yz}\,dA = P_y \quad \int_A y\sigma_{zz}\,dA = M_x - P_y(L-z)$$

$$\int_A \sigma_{zz}\,dA = P_z \quad \int_A (x\tau_{yz} - y\tau_{xz})\,dA = M_z. \tag{6a-f}$$

STRESS AND DEFORMATION FIELDS

In Saint-Venant extension, bending and torsion of an anisotropic beam, all of the stress components are independent of z. When flexure forces P_x and P_y are considered, then the normal stress σ_{zz} will vary linearly with z in accordance with global equilibrium and can be taken as:

$$\sigma_{zz} = \left\{\frac{P_x}{I_{yy}}x + \frac{P_y}{I_{xx}}y\right\}z + \sigma_{zz}^0(x, y) \tag{7}$$

where I_{xx} and I_{yy} are the area moments of inertia about the x and y axes, respectively, and σ_{zz}^0 is part of the stress related to extension, bending and torsion and satisfies eqns (4c–e),

$$\int_A x\sigma_{zz}^0\,dA = -M_y - P_x L, \quad \int_A y\sigma_{zz}^0\,dA = M_x - P_y L,$$

$$\int_A \sigma_{zz}^0\,dA = P_z, \tag{8a-c}$$

and the remaining five stresses are z-independent. In the absence of body forces, the stress equations of equilibrium can be cast into a form reflecting the quasi-two-dimensional nature of the stress state:

$$\frac{\partial\sigma_{xx}}{\partial x} + \frac{\partial\tau_{xy}}{\partial y} = 0,$$

$$\frac{\partial\tau_{xy}}{\partial x} + \frac{\partial\sigma_{yy}}{\partial y} = 0,$$

$$\frac{\partial\tau_{xz}}{\partial x} + \frac{\partial\tau_{yz}}{\partial y} + \frac{P_x}{I_{yy}}x + \frac{P_y}{I_{xx}}y = 0. \tag{9a-c}$$

The strain components in array $\{\varepsilon\}$ [eqn (1b)] can be divided into two parts, one which is entirely a function of (x, y) and the other reflecting the linear variation due to flexure forces. Using the constitutive relations (3b) in terms of the compliances S_{ij}, the strain components can be written as:

$$\{\varepsilon\} = \{\varepsilon^0\} - \{v\}\left\{\frac{P_x}{EI_{yy}}x + \frac{P_y}{EI_{xx}}y\right\}z \tag{10}$$

where $\{\varepsilon^0\}$ is a function of x and y only, and $E = 1/S_{33}$ is Young's modulus, which is

introduced here to abide by the more familiar elementary beam terminology. The array $\{v\}$ contains the cross-coupling coefficients whose components are

$$\{v\}^{\mathrm{T}} = \{v_1, v_2, -1, v_4, v_5, v_6\}, \tag{11a}$$

with

$$v_i = -\frac{S_{i3}}{S_{33}}, \tag{11b}$$

where v_1 and v_2 are the usual Poisson coefficients, and v_4, v_5, and v_6 express the three-dimensional extension–shear coupling that can occur in a completely anisotropic body.

To obtain the deformation quantities in terms of the extensional force, bending moments, torque and flexure forces, it is necessary to use the equilibrium equations (9a–c), strain–displacement relations (2a–f), the constitutive relations (3a–c) and the end-fixity conditions (5a–f). Omitting the very extensive algebraic details involved, the results for the displacement and strains are:

$$u = -\frac{P_x}{2EI_{yy}}\left\{\frac{z^2}{3}(z-3L) - \frac{v_4}{2}yz(z-2L) + \{v_1x^2 - v_2y^2\}(z-L)\right\} + \frac{1}{2EI_{yy}}\left\{M_y + \frac{v_4}{2}M_z\right\}z^2$$
$$-\theta yz - \frac{P_y}{2EI_{xx}}\left\{\{2v_1x + v_6y\}y(z-L) + \frac{v_5}{2}yz(z-2L)\right\} + \psi_x(x,y) \tag{12a}$$

$$v = -\frac{P_y}{2EI_{xx}}\left\{\frac{z^2}{3}(z-3L) - \frac{v_5}{2}xz(z-2L) + \{v_2y^2 - v_1x^2\}(z-L)\right\} - \frac{1}{2EI_{xx}}\left\{M_x + \frac{v_5}{2}M_z\right\}z^2$$
$$+\theta xz - \frac{P_x}{2EI_{yy}}\left\{\{v_6x + 2v_2y\}x(z-L) + \frac{v_4}{2}xz(z-2L)\right\} + \psi_y(x,y) \tag{12b}$$

$$w = -\frac{P_x}{2EI_{yy}}\{\{v_5x + v_4y\}x(z-L) - xz(z-2L)\} - \frac{1}{EI_{yy}}\left\{M_y + \frac{v_4}{2}M_z\right\}xz$$
$$+\frac{1}{EI_{xx}}\left\{M_x + \frac{v_5}{2}M_z\right\}yz - \frac{P_y}{2EI_{xx}}\{\{v_5x + v_4y\}y(z-L) - yz(z-2L)\}$$
$$-\frac{1}{EA}\left\{\frac{v_5}{2}P_x + \frac{v_4}{2}P_y - P_z\right\}z + \psi_z(x,y) \tag{12c}$$

and

$$\varepsilon_{xx} = -\frac{P_x v_1}{EI_{yy}}x(z-L) - \frac{P_y v_1}{EI_{xx}}y(z-L) + \frac{\partial \psi_x}{\partial x} \tag{13a}$$

$$\varepsilon_{yy} = -\frac{P_x v_2}{EI_{yy}}x(z-L) - \frac{P_y v_2}{EI_{xx}}y(z-L) + \frac{\partial \psi_y}{\partial y} \tag{13b}$$

$$\varepsilon_{zz} = -\frac{P_x}{2EI_{yy}}\{v_5x + v_4y + 2(L-z)\}x - \frac{P_y}{2EI_{xx}}\{v_5x + v_4y + 2(L-z)\}y$$
$$+\frac{1}{EI_{xx}}\left\{M_x + \frac{v_5}{2}M_z\right\}y - \frac{1}{EI_{yy}}\left\{M_y + \frac{v_4}{2}M_z\right\}x - \frac{1}{2EA}\{v_5P_x + v_4P_y - 2P_z\} \tag{13c}$$

$$\gamma_{yz} = -\frac{P_x}{EI_{yy}}\left\{\frac{v_6}{2}x + v_2y + v_4(z-L)\right\}x + \frac{P_y}{2EI_{xx}}\{(v_1x^2 - v_2y^2) - 2v_4y(z-L)\} + \theta x + \frac{\partial \psi_z}{\partial y} \tag{13d}$$

$$\gamma_{xz} = -\frac{P_x}{EI_{xx}}\left\{v_1 x + \frac{v_6}{2}y + v_5(z-L)\right\}y - \frac{P_x}{2EI_{yy}}\{(v_1 x^2 - v_2 y^2) + 2v_5 x(z-L)\} - \theta y + \frac{\partial \psi_z}{\partial x} \tag{13e}$$

$$\gamma_{yz} = -\frac{P_x v_6}{EI_{yy}}x(z-L) - \frac{P_x v_6}{EI_{xx}}y(z-L) + \frac{\partial \psi_x}{\partial y} + \frac{\partial \psi_y}{\partial x} \tag{13f}$$

where θ is the twist of the cross-section about the k axis and ψ_x, ψ_y and ψ_z are called the local deformations of the cross-section. These in-plane (ψ_x, ψ_y) and out-of-plane (ψ_z) local deformations must satisfy the following five conditions:

$$\frac{\partial \psi_x}{\partial x} - \{S_{11}\sigma_{xx} + S_{12}\sigma_{yy} + S_{13}\sigma_{zz}^0 + S_{14}\tau_{yz} + S_{15}\tau_{xz} + S_{16}\tau_{xy}\} = 0, \tag{14a}$$

$$\frac{\partial \psi_y}{\partial y} - \{S_{12}\sigma_{xx} + S_{22}\sigma_{yy} + S_{23}\sigma_{zz}^0 + S_{24}\tau_{yz} + S_{25}\tau_{xz} + S_{26}\tau_{xy}\} = 0, \tag{14b}$$

$$\frac{\partial \psi_x}{\partial y} + \frac{\partial \psi_y}{\partial x} - \{S_{16}\sigma_{xx} + S_{26}\sigma_{yy} + S_{36}\sigma_{zz}^0 + S_{46}\tau_{yz} + S_{56}\tau_{xz} + S_{66}\tau_{xy}\} = 0, \tag{14c}$$

$$\frac{\partial \psi_z}{\partial x} - \{S_{15}\sigma_{xx} + S_{25}\sigma_{yy} + S_{35}\sigma_{zz}^0 + S_{45}\tau_{yz} + S_{55}\tau_{xz} + S_{56}\tau_{xy}\} - \theta y - \frac{P_x}{2EI_{yy}}\{v_1 x^2 - v_2 y^2\} - \frac{P_y}{2EI_{xx}}\{2v_1 xy + v_6 y^2\} = 0, \tag{14d}$$

$$\frac{\partial \psi_z}{\partial y} - \{S_{14}\sigma_{xx} + S_{24}\sigma_{yy} + S_{34}\sigma_{zz}^0 + S_{44}\tau_{yz} + S_{45}\tau_{xz} + S_{46}\tau_{xy}\} + \theta x - \frac{P_x}{2EI_{yy}}\{2v_2 xy + v_6 x^2\} - \frac{P_y}{2EI_{xx}}\{v_2 y^2 - v_1 x^2\} = 0, \tag{14e}$$

where σ_{zz}^0 is given by:

$$\sigma_{zz}^0 = \{v_1\sigma_{xx} + v_2\sigma_{yy} + v_4\tau_{yz} + v_5\tau_{xz} + v_6\tau_{xy}\} - \frac{P_x}{2I_{yy}}\{v_5 x + v_4 y + 2L\}x - \frac{P_y}{2I_{xx}}\{v_5 x + v_4 y + 2L\}y - \frac{1}{A}\left\{\frac{v_5}{2}P_x + \frac{v_4}{2}P_y - P_z\right\} + \frac{1}{I_{xx}}\left\{M_x + \frac{v_5}{2}M_z\right\}y - \frac{1}{I_{yy}}\left\{M_y + \frac{v_4}{2}M_z\right\}x. \tag{14f}$$

The displacement relations (12a–c) can be viewed as that representing deformation of a beam of isotropic or orthotropic material plus additional contributions arising from anisotropic coupling. For example, the presence of v_4 and v_5 involve coupling of the flexure forces P_x and P_y with extension and twist, the extensional force P_z with shear in the y–z and x–z planes and the torque M_z with bending in the x–z and y–z planes. If v_4 and v_5 are absent, then the extension, bending and torsion problems can be studied independently of the flexure problem. Decoupling of these effects is possible if there is at least one plane of structural symmetry (monoclinic material) which must be the cross-section plane. The coefficient v_6 accounts for coupling of in-plane shear with the warpage of the cross-section. These observations of coupling behavior are in agreement with Wörndle (1982) for monoclinic materials, Tolf (1985) for orthotropic materials and Sokolnikoff (1946) for isotropic materials.

ANALYSIS OF THE LOCAL CROSS-SECTION DEFORMATIONS

The local deformation functions for an arbitrary-shaped cross-section are determined from variationally-derived algebraic equations based upon the minimum potential energy theorem along with two-dimensional finite element modeling of the cross-section. Although the displacement field is three-dimensional (12a–c), the functional form is explicit in the axial direction so that only the cross-section needs to undergo discretization. In this regard, it may be classified as a special case of the semi-analytical procedure reviewed by Zienkiewicz and Taylor (1987). This two-dimensional finite element modeling procedure has been applied successfully to the torsion of isotropic beams by Herrmann (1965), the flexure of isotropic beams by Mason and Herrmann (1968) and the flexure of monoclinic beams by Wörndle (1982).

The local deformations must be determined for seven cases (viz., three applied forces, three applied moments, twist rate). Standard isoparametric finite element methodology is employed so that most of the details can be omitted. Within the ith subregion of the cross-section, the displacement field can be written as:

$$\psi_x = [N_i(x,y)]\{\Psi_{x_i}\}, \quad \psi_y = [N_i(x,y)]\{\Psi_{y_i}\},$$
$$\psi_z = [N_i(x,y)]\{\Psi_{z_i}\}, \tag{15a–c}$$

where $[N_i(x,y)]$ is the bi-quadratic isoparametric interpolation function and $\{\Psi_{x_i}\}$, $\{\Psi_{y_i}\}$, and $\{\Psi_{z_i}\}$, are nodal displacements on the ith subregion boundary in the x, y and z directions, respectively. Substituting (15a–c) into (13a–f) gives $\{\varepsilon\}$ for the ith subregion in terms of generalized coordinates for the local deformations; ψ and the seven cases of $\{Q\}$.

$$\{\varepsilon_i\} = [B_i]\{\Psi_i\} + [\bar{F}_C]\{Q\} \tag{16}$$

where

$$[B_i]^{\mathrm{T}} = \begin{bmatrix} \dfrac{\partial[N_i(x,y)]}{\partial x} & 0 & 0 & 0 & 0 & \dfrac{\partial[N_i(x,y)]}{\partial y} \\ 0 & \dfrac{\partial[N_i(x,y)]}{\partial y} & 0 & 0 & 0 & \dfrac{\partial[N_i(x,y)]}{\partial x} \\ 0 & 0 & 0 & \dfrac{\partial[N_i(x,y)]}{\partial y} & \dfrac{\partial[N_i(x,y)]}{\partial x} & 0 \end{bmatrix} \tag{17a}$$

$$\{\Psi_i\}^{\mathrm{T}} = \{\{\Psi_{x_i}\}, \{\Psi_{y_i}\}, \{\Psi_{z_i}\}\} \tag{17b}$$

$$\{Q\}^{\mathrm{T}} = \{P_x, P_y, P_z, M_x, M_y, M_z, 0\} \tag{17c}$$

and $[F_C]$ is defined in the Appendix. Similarly, a matrix form of the displacements (12a–c) could also be defined in terms of the local deformations and $\{Q\}$.

The principle of minimum potential energy is given as

$$\delta\Pi = \sum_{i=1}^{n} \delta U_i - \delta W_e = 0 \tag{18}$$

where n is the total number of subregions, δU_i is the variation of the strain energy with respect to the local deformations of the ith subregion:

$$\delta U_i = \int_0^{L} \int_{A_i} \{\delta\varepsilon_i\}^{\mathrm{T}}[C]\{\varepsilon_i\}\, \mathrm{d}A_i\, \mathrm{d}z, \tag{19a}$$

and δW_e is the variation of the work of external forces of the ith subregion that results from the applied tractions on the beam ends:

$$\delta W_{e_i} = \int_{A_i} \{\tau_{xz}\delta\psi_x + \tau_{yz}\delta\psi_y + \sigma_{zz}\delta\psi_z\}|_{(z=L)}\,\mathrm{d}A_i$$

$$- \int_{A_i} \{\tau_{xz}\delta\psi_x + \tau_{yz}\delta\psi_y + \sigma_{zz}\delta\psi_z\}|_{(z=0)}\,\mathrm{d}A_i. \quad (19b)$$

A simplified form of this expression is obtained by making use of (3a–c) and (13a–f):

$$\delta W_{e_i} = \frac{P_x L}{I_{yy}} \int_{A_i} x\delta\psi_z\,\mathrm{d}A + \frac{P_y L}{I_{xx}} \int_{A_i} y\delta\psi_z\,\mathrm{d}A_i. \quad (20)$$

A set of linear algebraic equations for determining the local deformations in terms of $\{Q\}$ is obtained by substituting (16), (19a) and (20) into (18) and integrating over the beam volume. For the ith subregion, the set of equations have the form:

$$[K_i]\{\Psi_i\} = [[F_{W_i}] - [F_{C_i}]]\{Q\}, \quad (21)$$

where the stiffness matrix is defined as

$$[K_i] = L \int_{A_i} [B_i]^T [C][B_i]\,\mathrm{d}A_i \quad (22a)$$

and the force matrices are presented as

$$[F_{W_i}] = L \begin{bmatrix} 0 & 0 & 0 & 0 & 0 & 0 & 0 \\ 0 & 0 & 0 & 0 & 0 & 0 & 0 \\ \dfrac{1}{I_{yy}} \displaystyle\int_{A_i} x[N_i(x,y)]\,\mathrm{d}A_i & \dfrac{1}{I_{xx}} \displaystyle\int_{A_i} y[N_i(x,y)]\,\mathrm{d}A_i & 0 & 0 & 0 & 0 & 0 \end{bmatrix} \quad (22b)$$

and

$$[F_{C_i}] = L \int_{A_i} [B_i]^T [C][\bar{F}_{C_i}]\,\mathrm{d}A_i, \quad (22c)$$

with $[\bar{F}_{C_i}]$ also being defined in the Appendix. A closer examination of (21), (22) and (A3) reveals that the local deformations for the applied flexural forces P_x and P_y are beam length L dependent, while the local deformations for the remaining five cases are independent of the beam length.

The equations for the ith subregion (21) are assembled into a complete model of the cross-section using standard finite element procedures. Unit solutions for the local deformations (ψ_x, ψ_y, ψ_z) can be calculated for the seven cases by setting each of the seven coordinates of $\{Q\}$ equal to unity and the remaining six to zero. Write the calculated local deformations for the ith subregion as

$$\{\Psi_i\} = [\bar{\Psi}_i]\{Q\}, \quad (23)$$

where each of the seven columns of $[\bar{\Psi}_i]$ are the unit local deformations associated with the seven cases of $\{Q\}$. The dimensional units of the first three columns are length per unit force, the next three columns are length per unit moment, and the units for the last column are length per unit twist rate. Similarly, the stress components of the ith subregion can be written in terms of the seven cases as:

$$\{\sigma_i\} = [\overline{\sigma_i}]\{Q\}, \tag{24a}$$

where

$$[\overline{\sigma_i}] = [C][[B_i][\overline{\Psi_i}] + [\overline{F_{C_i}}]]. \tag{24b}$$

The desired form of the results for the local deformations should involve the three applied forces and the three applied moments only. Thus, the twist rate (θ) needs to be expressed in terms of these forces and moments. To this end, substitute the 4th and 5th eqns of (24a) into (4f), integrate over the n cross-section subregions, and then rearrange to get:

$$Q_7 = \theta = a_1 P_x + a_2 P_y + a_3 P_z + a_4 M_x + a_5 M_y + a_6 M_z, \tag{25a}$$

where

$$a_k = -\frac{\overline{a_k}}{\overline{a_7}}, \quad (k = 1\text{–}5) \tag{25b}$$

$$a_6 = \frac{1 - \overline{a_6}}{\overline{a_7}}, \tag{25c}$$

and

$$a_k = \sum_{i=1}^{n} \int_{A_i} \{x_i(\sigma_{3k})_i - y_i(\sigma_{5k})_i\}\, dA_i, \quad (k = 1, 7). \tag{25d}$$

Finally, the local deformation functions can be written in terms of the three applied forces and three applied moments by combining eqns (23) and (25a):

$$\{\Psi_i\} = [\overline{\Psi_i}][T]\{\bar{Q}\}, \tag{26a}$$

with

$$[T] = \begin{bmatrix} 1 & 0 & 0 & 0 & 0 & 0 \\ 0 & 1 & 0 & 0 & 0 & 0 \\ 0 & 0 & 1 & 0 & 0 & 0 \\ 0 & 0 & 0 & 1 & 0 & 0 \\ 0 & 0 & 0 & 0 & 1 & 0 \\ 0 & 0 & 0 & 0 & 0 & 1 \\ a_1 & a_2 & a_3 & a_4 & a_5 & a_6 \end{bmatrix} \tag{26b}$$

and

$$\{\bar{Q}\}^T = \{P_x, P_y, P_z, M_x, M_y, M_z\}. \tag{26c}$$

Similar relations for the stress distribution can be developed by combining (24a) and (26b)

$$\{\sigma_i\} = [\bar{\sigma}_i][T]\{\bar{Q}\}. \tag{27}$$

BEHAVIOR OF AN ANISOTROPIC BEAM

The general behavior of a cantilever beam having an arbitrary cross-section and rectilinear anisotropy will be addressed in two examples. The first example will investigate the behavior that results from extension, bending and twist only, while the second example will address flexure and its coupling with the other three Saint-Venant solutions.

Extension, bending and torsion

Applying an extension force P_z through the centroid of the cross-section will produce a twist rate ($\theta = a_3 P_z$) according to eqn (25a) and displacements of the form [from eqn (12a–c)]:

$$u = -a_3 P_z yz + \psi_x,$$
$$v = a_3 P_z xz + \psi_y,$$
$$w = \frac{P_z}{EA} z + \psi_z. \tag{28a–c}$$

From eqns (14a–e) it is straightforward to show that $a_3 = 0$, since there is no twisting of a homogeneous anisotropic cantilever beam as a result of applied extension and thus:

$$\psi_x = \bar{\psi}_x^{(3)} P_z = \frac{P_z}{EA}\left(v_1 x + \frac{v_6}{2} y\right),$$
$$\psi_y = \bar{\psi}_y^{(3)} P_z = \frac{P_z}{EA}\left(v_2 y + \frac{v_6}{2} x\right),$$
$$\psi_z = \bar{\psi}_z^{(3)} P_z = \frac{P_z}{EA}(v_5 x + v_4 y), \tag{29a–c}$$

where the superscript (3) is associated with the third column of the local deformation matrix in eqn (23).

Applying a bending moment M_x will produce bending and twisting ($\theta = a_4 M_x$), where:

$$u = -a_4 M_x yz + \psi_x$$
$$v = -\frac{M_x}{2EI_{xx}} z^2 + a_4 M_x xz + \psi_y$$
$$w = \frac{M_x}{EI_{xx}} yz + \psi_z. \tag{30a–c}$$

Again integrating eqns (14a–e) it can be shown that:

$$a_4 = \frac{v_5}{2EI_{xx}}$$
$$\psi_x = (\bar{\psi}_x^{(4)} + a_4 \bar{\psi}_x^{(7)}) M_x = -\frac{M_x}{2EI_{xx}}(v_6 y^2 + 2v_1 xy),$$
$$\psi_y = (\bar{\psi}_y^{(4)} + a_4 \bar{\psi}_y^{(7)}) M_x = \frac{M_x}{2EI_{xx}}(v_1 x^2 - v_2 y^2),$$
$$\psi_z = (\bar{\psi}_z^{(4)} + a_4 \bar{\psi}_z^{(7)}) M_x = -\frac{M_x}{2EI_{xx}}(v_5 xy + v_4 y^2), \tag{31a–d}$$

where the superscripts (4) and (7) correspond to the fourth and seventh columns of the local deformation matrix in eqn (23). Similar relations can be developed for an applied bending moment M_y, where the twisting of the beam is defined as ($\theta = a_5 M_y$) with

$$a_5 = \frac{v_4}{2EI_{yy}}. \tag{32}$$

Applying an axial force P_3 that is offset from the centroid will produce extension, bending and twist. However, there exists an infinite number of points that form a line within the cross-section, which will be called the "*line of extension–bending centers*", where the application of an axial force will produce beam bending with no twisting ($\theta = 0$). The definition of this line, which passes through the centroid, can be calculated by applying P_3 at a point (x_e, y_e) and noting that the equivalent centroidal forces and moments are equal to:

$$P_z = P_3, \quad M_x = y_e P_3, \quad M_y = -x_e P_3. \tag{33a–c}$$

Substituting eqns (33a–c), (31a) and (32) into (25a) and noting that ($\theta = 0$), the line of extension–bending centers is found to be:

$$y_e = \frac{a_5}{a_4} x_e = \frac{v_4}{v_5} \frac{I_{xx}}{I_{yy}} x_e, \tag{34}$$

and this line is the x-axis for $v_4 = 0$, the y-axis for $v_5 = 0$, and the entire cross-section x–y plane if $v_4 = v_5 = 0$.

The bending–torsion coupling behavior can be studied by further making use of (25a). For example, the application of M_z will produce beam twisting of the form:

$$GJ\theta = M_z \tag{35a}$$

where $GJ = 1/a_6$ and bending, where the displacement of the centroidal axis in the x–z and y–z planes, can be characterized by [from (12a–c)]

$$u = \left\{\frac{v_4 M_z}{4EI_{yy}}\right\} z^2 \quad \text{and} \quad v = -\left\{\frac{v_5 M_z}{4EI_{xx}}\right\} z^2, \tag{35b,c}$$

respectively. In order to produce a state of pure twist ($u = v = 0$), constraint bending moments must be applied, where

$$M_x = -\left\{\frac{v_5}{2}\right\} M_z \quad \text{and} \quad M_y = -\left\{\frac{v_4}{2}\right\} M_z. \tag{36a,b}$$

This is equivalent to applying a couple (M_3) about a vector that is skew to the cross-section normal, where the vector is defined as

$$e_3 = -\left\{\frac{v_5}{2}\right\} i - \left\{\frac{v_4}{2}\right\} j + \{1\} k. \tag{37}$$

An anisotropic cross-section torsion stiffness (GJ_a) that is based upon pure beam twist (instead of a torsion moment; M_z) can be defined by substituting eqns (36a,b), (31a) and (32) into eqn (25a) and rearranging

$$GJ_a\theta = M_z, \tag{38a}$$

where

$$GJ_a = \frac{GJ}{1 - \dfrac{GJ}{EI_{yy}}\left(\dfrac{v_4}{2}\right)^2 - \dfrac{GJ}{EI_{xx}}\left(\dfrac{v_5}{2}\right)^2}, \tag{38b}$$

and $GJ_a \geqslant GJ$.

To place the cantilever beam in pure bending, without twist, the three moments have to be applied properly. For example, to produce beam bending in the x–z plane only ($v = \theta = 0$), the relative magnitudes of the applied moments are determined by setting eqns (12b) and (25a) to zero and then combining to form a couple (M_z) that acts about a vector e_z equal to

$$e_z = -\left\{\frac{v_4 v_5}{\dfrac{EI_{yy}}{EI_{xx}}v_5^2 - \dfrac{4EI_{yy}}{GJ}}\right\}i + \{1\}j + \left\{\frac{2v_4}{\dfrac{EI_{yy}}{EI_{xx}}v_5^2 - \dfrac{4EI_{yy}}{GJ}}\right\}k. \tag{39}$$

Substituting M_z into eqn (12a), one can determine a simplified bending displacement equation in terms of an effective anisotropic bending stiffness:

$$u = \frac{M_z}{2EI_{yy_a}}z^2, \tag{40a}$$

where

$$EI_{yy_a} = EI_{yy}\left[\frac{1 - \dfrac{GJ}{EI_{xx}}\left(\dfrac{v_5}{2}\right)^2}{1 - \dfrac{GJ}{EI_{xx}}\left(\dfrac{v_5}{2}\right)^2 - \dfrac{GJ}{EI_{yy}}\left(\dfrac{v_4}{2}\right)^2}\right] \tag{40b}$$

and $EI_{yy_a} > EI_{yy}$ for non-zero values of v_4. Similar relations can be easily developed for bending in the y–z plane where $EI_{xx_a} > EI_{xx}$ for non-zero values of v_5.

The "*center of twist*" is defined as a point (x_t, y_t) within the tip cross-section plane for which the in-plane displacements (u, v) are zero when the beam is subjected to (M_z) only. The coordinates of this point are found by setting the displacements (u, v) and in eqns (12a–b) to zero and making use of eqns (23), (25c) and (35a):

$$x_t = \frac{v_5 L}{4}\frac{GJ}{EI_{xx}} - \frac{GJ}{L}\left\{\Psi_v^{(6)}(x_t, y_t) + \frac{1}{GJ}\Psi_v^{(7)}(x_t, y_t)\right\}, \tag{41a}$$

$$y_t = \frac{v_4 L}{4}\frac{GJ}{EI_{yy}} + \frac{GJ}{L}\left\{\Psi_v^{(6)}(x_t, y_t) + \frac{1}{GJ}\Psi_v^{(7)}(x_t, y_t)\right\}, \tag{41b}$$

where $\Psi_v^{(6)}(x_t, y_t)$, $\Psi_v^{(6)}(x_t, y_t)$, $\Psi_v^{(7)}(x_t, y_t)$ and $\Psi_v^{(7)}(x_t, y_t)$ are the magnitudes of the unit local deformations at the twist center as a result of an applied twist moment (M_z) and applied twist (θ), respectively. Since the coordinates (x_t, y_t) appear on both sides of eqns (41a,b), this location must be determined by iteration.

Flexure

The coupling between the applied flexural forces and beam twist can be used to locate a point in the tip cross-section plane commonly called the *shear* (*or flexural*) center. Using the definition that "any flexural force that acts through this point will produce beam bending without twist ($\theta = 0$)", one can apply a general flexural force (P_{xs}, P_{ys}) that acts through this point (Fig. 2) and recognize that the equivalent forces and moments at the centroid are

$$P_x = P_{xs}, \quad P_y = P_{ys}, \quad M_z = P_{ys}x_s - P_{xs}y_s, \tag{42a–c}$$

where x_s and y_s are the unknown locations of the shear center. Thus, the location is determined by substituting eqn (41a–c) into eqn (25a) and noting that ($\theta = 0$); thus

$$x_s = -\frac{a_2}{a_6} = -\frac{\overline{a_2}}{1-\overline{a_6}}, \quad y_s = \frac{a_1}{a_6} = \frac{\overline{a_1}}{1-\overline{a_6}}. \tag{43a,b}$$

For beams that exhibit less than generally-anisotropic behavior ($v_4 = v_5 = 0$), $\overline{a_6}$ will equal zero and the above equations reduce to those presented by Sokolnikoff (1946) for isotropic cross-sections. For homogeneous cross-sections composed of either isotropic or anisotropic materials, the center of twist and the shear center are coincident as proven by Reissner and Tsai (1972).

NUMERICAL RESULTS

Two sets of numerical results are presented to illustrate how variations in cross-section geometry, beam length and material definition affect the behavior of the cantilever beam. In the first set, beams having solid elliptical cross-sections with aspect ratios that range from thick ($a/b = 0.1$) to circular ($a/b = 1$) to thin ($a/b = 2$, 10) were analyzed. In the second set, beams having thin ($t/c = 0.1$) circular arc sections were studied, where the included arc angle (2β) varies from 0° (flat rectangle) to 180° (semi-circle). This second set of cross-sections was selected because circular arc sections are representative of cambered sections (for 10% camber; $2\beta \approx 45°$) commonly found in aerospace applications. Examples

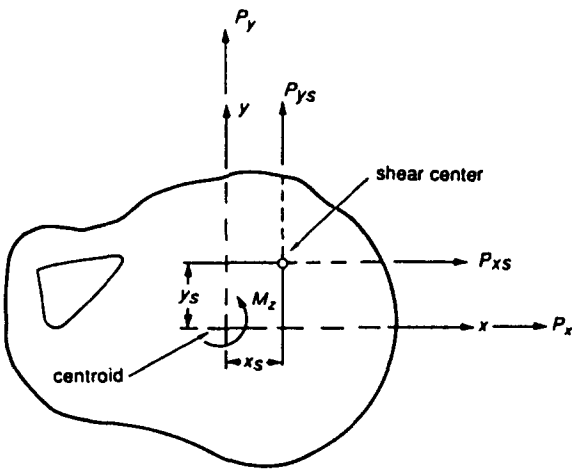

Fig. 2. Beam cross-section and shear center location.

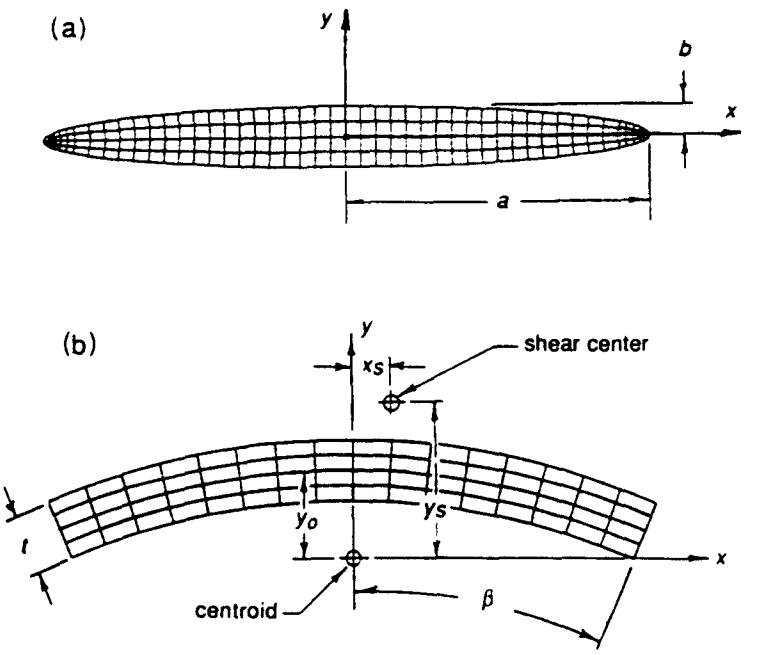

Fig. 3. Finite element discretization of (a) thin elliptical cross-section ($a/b = 10$), and (b) thin circular arc section ($c/t = 10$, $2\beta = 45°$).

of typical finite element mesh definitions for the thin elliptical ($a/b = 10$) and circular arc ($2\beta = 45°$) sections are presented in Figs 3a,b.

The beam material is assumed to be composed of a single set of unidirectional composite fibers (T300/5208 graphite/epoxy). The properties of the fiber system (Table 1) are defined relative to an orthogonal reference frame (1, 2, 3) where the 1-axis is coincident with the fiber direction. Aligning the fiber axes with (x, y, z) will produce orthotropic beam behavior with $v_4 = v_5 = v_6 = 0$. Complete anisotropic behavior can be observed for fiber sets that are not aligned with (x, y, z). Three orientation angles (θ_x, θ_y, θ_z) are used to locate the (1, 2, 3) relative to (x, y, z), where a positive angle is defined as a counterclockwise rotation about the corresponding Cartesian axis.

Complicated trigonometric relationships exist between (θ_x, θ_y, θ_z) and the coefficients (v_1–v_6). These relations can be simplified if the orientation angles are studied one at a time. For example, rotating the fibers, which are initially aligned with z, about y (θ_y) will result in the following non-zero coefficients:

$$v_1 = \frac{v_{12}(\cos^4\theta_y + \sin^4\theta_y) - \left(1 + \left(\frac{E_{11}}{E_{22}}\right) - \left(\frac{E_{11}}{G_{12}}\right)\right)\cos^2\theta_y \sin^2\theta_y}{\left\{\cos^4\theta_y + \left(\frac{E_{11}}{E_{22}}\right)\sin^4\theta_y + \left(\frac{E_{11}}{G_{12}} - 2v_{12}\right)\cos^2\theta_y \sin^2\theta_y\right\}}, \tag{44a}$$

$$v_2 = \frac{v_{13}\cos^2\theta_y + v_{23}\left(\frac{E_{11}}{E_{22}}\right)\sin^2\theta_y}{\left\{\cos^4\theta_y + \left(\frac{E_{11}}{E_{22}}\right)\sin^4\theta_y + \left(\frac{E_{11}}{G_{12}} - 2v_{12}\right)\cos^2\theta_y \sin^2\theta_y\right\}}, \tag{44b}$$

Table 1. Material properties of T300/5208 graphite/epoxy

E_{11}	132.3 GPa
$E_{22} = E_{33}$	10.75 GPa
$G_{12} = G_{13} = G_{23}$	5.65 GPa
$v_{12} = v_{13}$	0.239
v_{23}	0.400

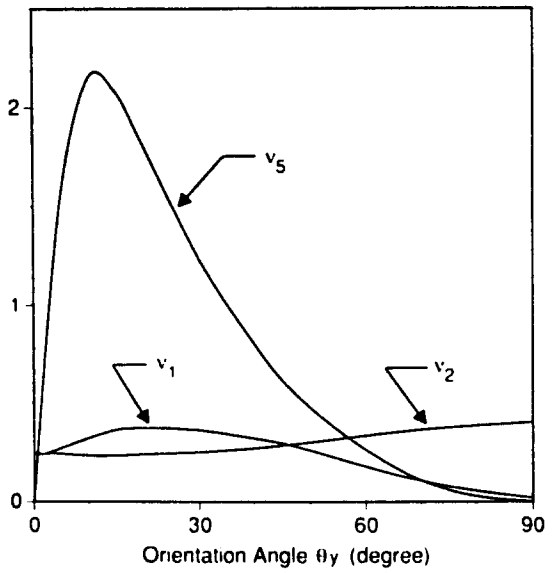

Fig. 4. Variation of Poisson and coupling coefficients with θ_y orientation for T300/5208 graphite/epoxy fibers initially aligned with the z axis of the beam.

$$v_5 = -\frac{2\left(\left(1+v_{12}-\left(\frac{E_{11}}{2G_{12}}\right)\right)\cos^2\theta_y-\left(v_{12}+\left(\frac{E_{11}}{E_{22}}\right)-\left(\frac{E_{11}}{2G_{12}}\right)\right)\sin^2\theta_y\right)\cos^2\theta_y\sin^2\theta_y}{\left\{\cos^4\theta_y+\left(\frac{E_{11}}{E_{22}}\right)\sin^4\theta_y+\left(\frac{E_{11}}{G_{12}}-2v_{12}\right)\cos^2\theta_y\sin^2\theta_y\right\}}, \tag{44c}$$

where the 3-axis and y remain coincident. The variation of v_1, v_2 and v_5 as a function of θ_y is presented in Fig. 4, with v_5 reaching its maximum at 12°. Similarly, introducing a rotation of the fiber set in the y–z plane (θ_x rotation) results in a non-zero value of v_4 with both v_5 and v_6 equal to zero. The v_1, v_2 and v_4 relations for a θ_x rotation are equal to v_2 [from eqn (44b)], v_1 [from eqn (44a)] and $-v_5$ [from eqn (44c)], respectively, when θ_y is replaced with θ_x, and the indices (2) and (3) are exchanged. In order to introduce a non-zero value of v_6 (with $v_4 = v_5 = 0$), the fibers (1-axis) are initially aligned with x and then the fiber system is rotated about z (θ_z), so that z and the 3-axis remain coincident, thus

$$v_1 = \left(v_{13}\left(\frac{E_{33}}{E_{11}}\right)\cos^2\theta_z+v_{23}\left(\frac{E_{33}}{E_{22}}\right)\sin^2\theta_z\right), \tag{45a}$$

$$v_2 = \left(v_{23}\left(\frac{E_{33}}{E_{22}}\right)\cos^2\theta_z+v_{13}\left(\frac{E_{33}}{E_{11}}\right)\sin^2\theta_z\right), \tag{45b}$$

$$v_6 = 2\left(v_{13}\left(\frac{E_{33}}{E_{11}}\right)-v_{23}\left(\frac{E_{33}}{E_{22}}\right)\right)\cos\theta_z\sin\theta_z. \tag{45c}$$

Elliptical cross-section

The effect of cross-section geometry and material definition on beam behavior was studied by analyzing four different homogeneous cantilever beams of length ($L/a = 10$), where the aspect ratios of the solid elliptical cross-sections range from thick ($a/b = 0.1$) to circular ($a/b = 1$) to thin ($a/b = 2$, 10). Changes in the material property definition were introduced by rotating the fiber set in the x–z plane (θ_y, introduce v_5, Fig. 4) and in the

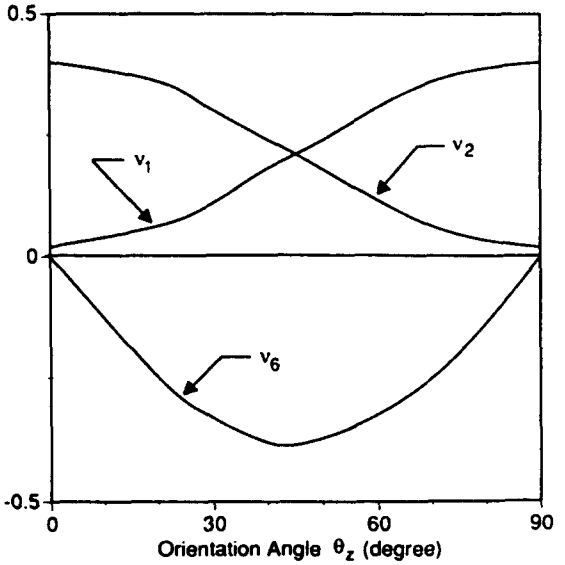

Fig. 5. Variation of Poisson and coupling coefficients with θ_z orientation for T300/5208 graphite/epoxy fibers initially aligned with the x axis of the beam.

x–y plane (vary θ_z, introduce v_6, Fig. 5). Rotating the fibers in the y–z plane (θ_x, v_4) was not investigated, since the results from rotations in the x–z plane are directly applicable.

The variations in the torsion stiffness [GJ, eqn (35a)] and the anisotropic torsion stiffness [GJ_a, eqn (38b)] as a function of fiber orientation in the x–z plane (θ_y) and the cross-section aspect ratio (a/b) are presented in Fig. 6, where these results have been normalized to the torsion stiffness of an elliptical cross-section having uniaxial fibers:

$$GJ_0 = G_{23}\pi \frac{a^3 b^3}{a^2 + b^2}. \tag{46}$$

Both of the section constants, GJ and GJ_a, are highly dependent upon the orientation

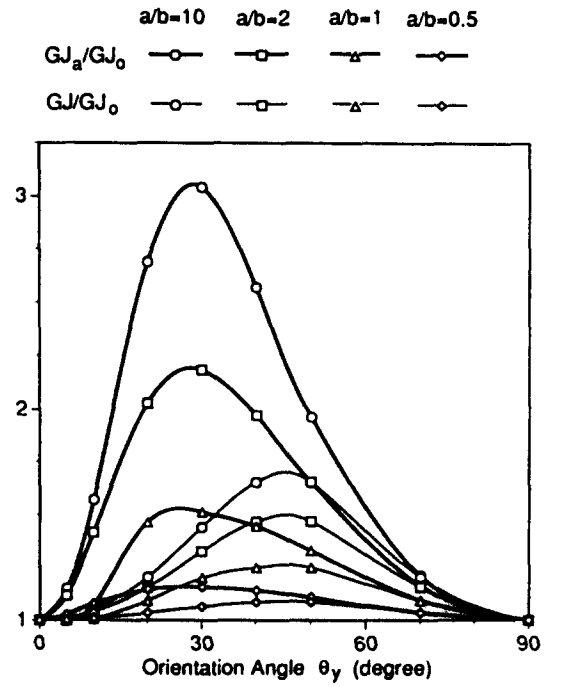

Fig. 6. Anisotropic torsion stiffness (GJ_a) and torsion stiffness (GJ) of elliptical cross-sections as a function of θ_y fiber orientation.

angle θ_y, where GJ and GJ_a reach relative maximums at 45° and 30°, respectively, independent of a/b. The curve associated with GJ_a creates an upper envelope for the GJ curve for a given value of a/b, where the two are effectively equal as v_5 approaches 0 ($\theta_y \geq 70°$). For a given non-zero value of θ_y, the torsion constants for a thin cross-section experience a much larger increase than a thick section, as a result of a large GJ/EI_{xx} ratio. For example, GJ/EI_{xx} is 100 times larger for $a/b = 10$ than for $a/b = 0.1$. Thus for thin sections, rotating the fibers in the plane of the major cross-section dimension (a) can have a profound effect while rotating the fibers in the minor direction (b) will produce a negligible increase, since $GJ/EI_{xx} \gg GJ/EI_{yy}$.

The line of extension centers is coincident with the x axis for fibers orientated with the x–z plane (θ_y with $v_4 = 0$). This is easily understood from classical laminated plate theory [see Jones (1975)], since offsetting an axial force in the x direction produces an effective bending moment M_y which acts about a vector orthogonal to the fiber plane and thus will not influence twist ($\theta = 0$). Furthermore, offsetting an axial force in the y direction produces an effective bending moment M_x acting in the fiber plane, that produces twist. Similarly, rotating the fibers with the y–z plane (θ_x with $v_5 = 0$) will result in the line of extension centers being coincident with the y-axis. Finally, the line of extension centers is the x–y plane if the fibers are rotated within the cross-section plane (θ_z with $v_4 = v_5 = 0$).

The movement of the shear center in the x direction ($x_s/2a$) as a function of fiber orientation in the x–z plane (θ_y) and aspect ratio (a/b) is presented in Fig. 7. These results illustrate that: (1) thin cross-sections (large a/b) can experience large movements ($x_s \approx 18a$), (2) the shear center will lie outside of the cross-section for almost all non-zero values of rotation ($5° < \theta_y < 75°$), and (3) the maximum movement generally occurs for values of θ_y near 30° for thick sections and 35° for thin sections. Rotating the fibers in the x–z plane with a value of $(-\theta_y)$ will produce identical movements but in the $-x$ direction. Furthermore, the shear center location is linearly dependent upon beam length for material configurations having non-zero values of either v_4 or v_5. Otherwise, the shear center is independent of beam length for either isotropic or a restricted class ($v_6 \neq 0$, $v_4 = v_5 = 0$) of orthotropic materials.

Thin circular arc sections

A second set of homogeneous cantilever beams of length ($L/c = 10$) having thin ($t/c = 0.1$) circular arc sections was analyzed, where c is the mid-line length of the arc cross-section. This study investigated changes in the cross-section properties as a result of varying the included arc angle (2β) from 0° (flat rectangle) to 180° (semi-circle) and varying the

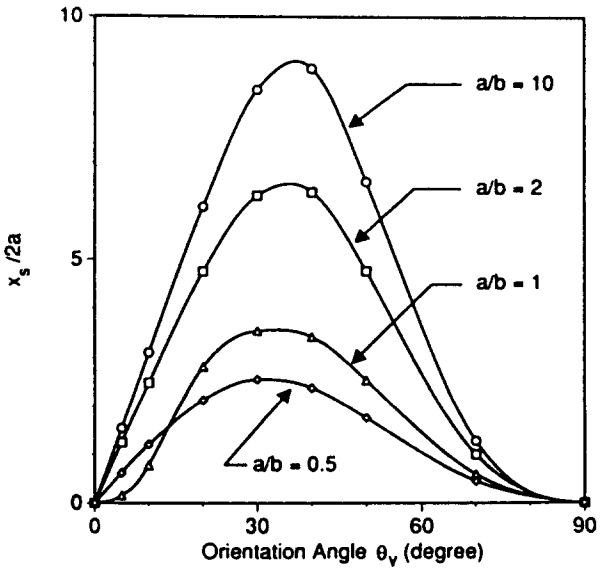

Fig. 7. Shear center location (x_s) of elliptical cross-sections as a function of θ_y fiber orientation.

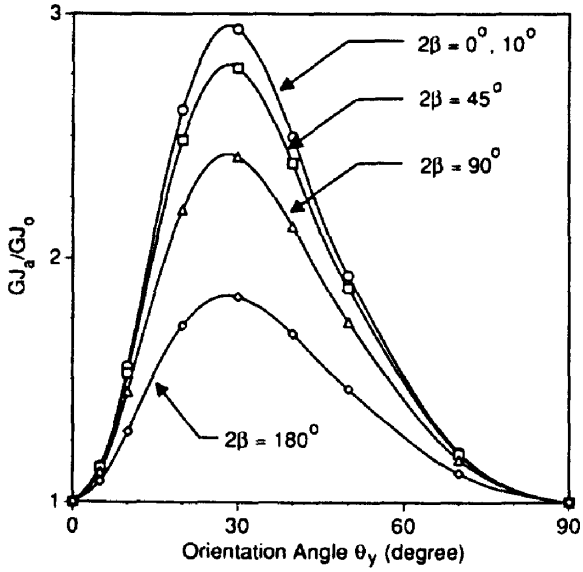

Fig. 8. Anisotropic torsion stiffness (GJ_a) of thin circular arc sections as a function of θ_y fiber orientation.

material property definition by rotating the fiber set in the x–z plane (θ_y, v_5, Fig. 4). This cross-section is of interest because for non-zero included angles, β, the centroid is located inside the mid-line of the arc section, whereas the shear center is located, in general, outside of the arc mid-line.

The variations in the anisotropic torsion stiffness (GJ_a) and the torsion stiffness (GJ) as a function of orientating the fiber direction in the x–z plane (θ_y) and varying the included angle (2β) are presented in Figs 8 and 9, respectively. The results are normalized using the torsion stiffness of a thin rectangular cross-section with uniaxial fibers:

$$GJ_0 = G_{23}kct^3 \tag{47}$$

where $k = 0.312$ for $t/c = 0.10$. From Fig. 8, GJ_a for slightly-curved arc sections ($2\beta < 10^\circ$) is dependent upon θ_y (v_5) only, since I_{xx} is effectively constant, whereas for highly-curved sections the dependency on θ_y is much less, since I_{xx} has increased. Comparing Figs 8 and 9, the torsion constant (GJ) is always lower than (GJ_a) for a given orientation angle and

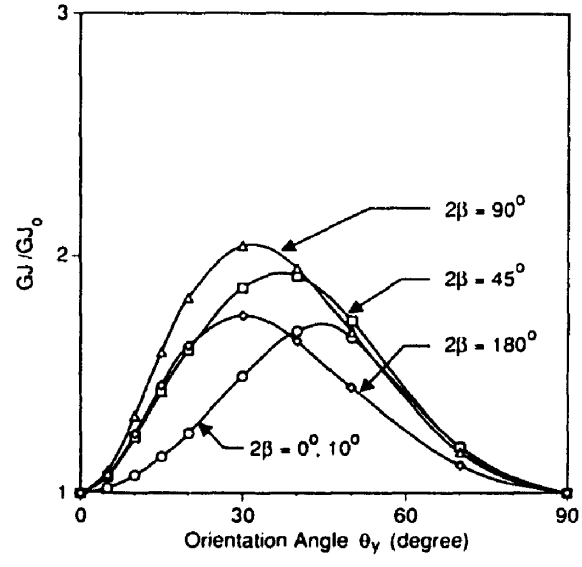

Fig. 9. Torsion stiffness (GJ) of thin circular arc sections as a function of θ_y fiber orientation.

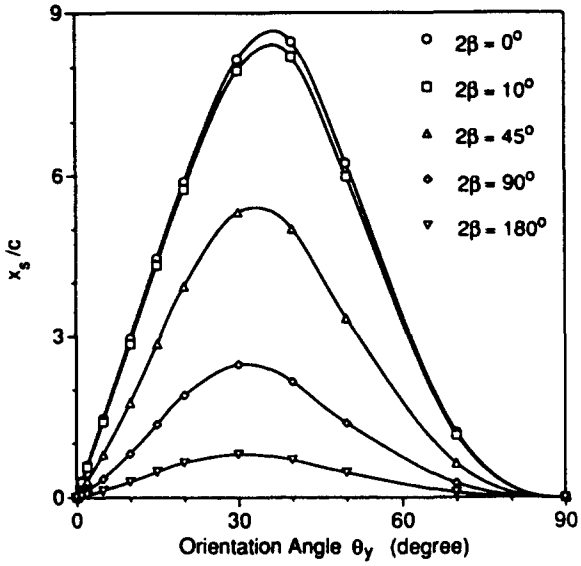

Fig. 10. Shear center location (x_s) of thin circular arc sections as a function of θ_y fiber orientation.

included angle. As (2β) is increased from 0° to 90°, the magnitude of (GJ_d) steadily decreases while the value of (GJ) significantly increases and its maximum shifts from $\theta_y = 45°$ to $\theta_y = 30°$. However, for ($2\beta > 90°$), (GJ_d) further decreases because of increasing I_{xx} and (GJ) now decreases to remain less than (GJ_d).

The x and y direction locations of the shear center as a result of varying the material orientation angle θ_y and the included arc angle (2β) are presented in Figs 10–12. The x direction distance of the shear center from the centroid (x_s/c) is presented in Fig. 10. As the included angle of the arc is increased from a slight curve ($2\beta \approx 0°$, 10°) to a semi-circle ($2\beta = 180°$), the maximum (x_s) distance is reduced by a factor of 10. This maximum distance occurs at $\theta_y = 35°$ for slightly-curved arcs and $\theta_y = 30°$ for a semi-circular arc. Furthermore, for the current beam length ($L/c = 10$), the shear center is located well outside of the section planform for almost all included angles and fiber orientations. In Fig. 11, the y direction distance of the shear center from the centroid is presented, where the results are normalized to the results for a homogeneous isotropic arc section:

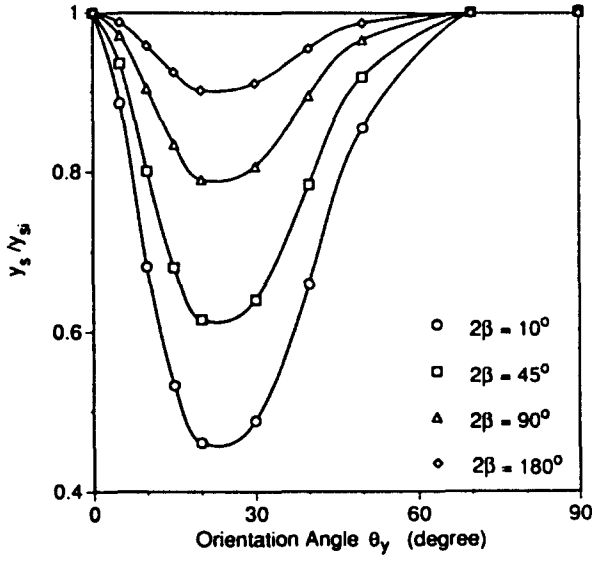

Fig. 11. Shear center location (y_s) of thin circular arc sections as a function of θ_y fiber orientation.

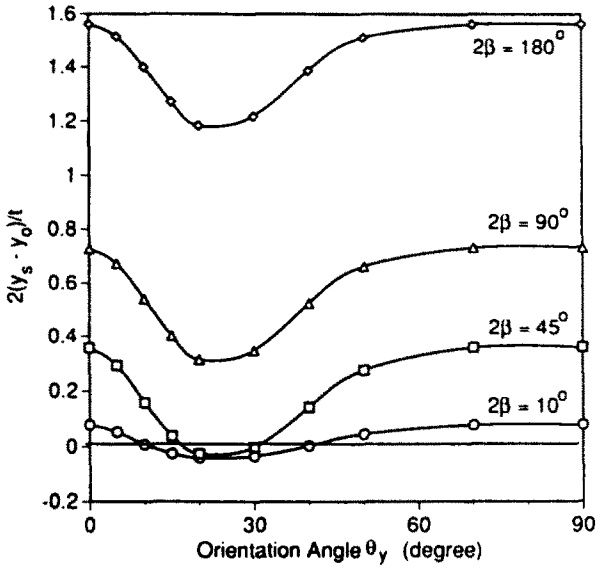

Fig. 12. Shear center location measured from the mid-line of the arc section ($y_s - y_0$) as a function of θ_y fiber orientation.

$$y_{s_0} = c\frac{(\sin^2\beta - 2\beta^2)\cos\beta + \beta\sin\beta}{2\beta^2(\beta - \cos\beta\sin\beta)}. \tag{48}$$

The reduction in the y direction offset can be significant for fiber angles less than 70° where this effect is more pronounced in slightly-curved arc sections ($2\beta \leqslant 10°$) than in highly-curved arc sections. For fiber directions where v_5 is negligible, the y direction shear center offset is identical to the isotropic prediction. These results are presented in an alternate form (see Fig. 12) as the y direction shear center distance measured from the mid-line of the arc section ($y_s - y_0$) normalized to one-half of the section thickness ($t/2$). These results illustrate that for slightly- to moderately-curved arc sections ($2\beta \leqslant 45°$) it is possible to locate the shear center on the inside of the arc mid-line and nearer to the centroid by properly selecting the fiber orientation angle. For highly-curved arc sections, it is possible to locate the shear center closer to the arc mid-line, but it is not possible to locate it on the inside of this arc-line.

CONCLUSIONS

An analytical model has been developed for determining the displacement and stress distributions to the Saint-Venant extension, bending, torsion and flexure problems for a homogeneous prismatic anisotropic beam with an arbitrary cross-section. The principle of minimum potential energy was applied to a discretized representation of the cross-section to determine the local deformations in-plane and warping out of the section plane. All of the properties that define the behavior of the anisotropic section have been developed, including the shear center, tension center and the center of twist. A new geometric parameter, the line of extension centers, is presented, which passes through the centroid and has a slope equal to $(v_4 I_{xx})/(v_5 I_{yy})$. A numerical analysis of four cantilever beams having different elliptical cross-sections and lengths revealed that: (1) the anisotropic torsion constant (GJ_a) reaches a relative maximum at a fiber direction of (30°) whereas (GJ) reaches a maximum at (45°), (2) for thin sections, rotating the fibers in the plane that includes the major section dimension can have profound effects on the torsion stiffness, (3) the shear center location is a beam length-dependent property if either v_4 or v_5 exist (rotation of the material fibers about the x or y axes), and (4) the shear center will lie well outside of the section planform for thin sections. A second numerical study of thin circular arc sections showed that: (1) increasing the included arc angle (camber) will increase (GJ) and decrease (GJ_a) up to

($2\beta = 90^\circ$) independent of material definition because of increasing I_{xx}, (2) increasing the included arc angle from 0° to 180° will greatly reduce the maximum x direction shear center offset, and (3) for slightly- to moderately-curved arc section ($2\beta \leqslant 45^\circ$), it is possible to locate the shear center inside of the arc mid-line (y direction) by properly selecting the fiber orientation angle.

REFERENCES

Bauchau, O. A. (1985). A beam theory for anisotropic materials. *ASME J. Appl. Mech.* **52**, 416–422.

Giavotto, V., Borri, M., Mantegazza, P. and Ghiringhelli, G. (1983). Anisotropic beam theory and applications. *Comput. Struct.* **16**(1–4), 403–413.

Goetschel, D. B. and Hu, T. H. (1985). Quantification of Saint-Venant's principle for a general prismatic member. *Comput. Struct.* **21**(5), 869–874.

Herrmann, L. R. (1965). Elastic torsional analysis of irregular shapes. *J. Engng Mech. Div. ASCE* **91**(EM6), 11–19.

Iesan, D. (1976). Saint-Venant's problem for inhomogeneous and anisotropic elastic bodies. *J. Elasticity* **6**(3), 277–294.

Jones, R. M. (1975). *Mechanics of Composite Materials*. Hemisphere, New York.

Kosmatka, J. B. (1986). Structural dynamic modeling of advanced composite propellers by the finite element method. Ph.D. Dissertation, University of California, Los Angeles.

Kosmatka, J. B. and Friedmann, P. P. (1989). Vibration analysis of composite turbo-propellers using a nonlinear beam-type finite element approach. *AIAA Jl* **27**(11), 1606–1615.

Lekhnitskii, S. G. (1963). *Theory of Elasticity of an Anisotropic Body*. Holden-Day, San Francisco.

Mason, W. E. and Herrmann, L. R. (1968). Elastic shear analysis of general prismatic shaped beams. *J. Engng Mech. Div. ASCE* **94**(EM4), 965–983.

Mindlin, R. D. (1975). Solution of St Venant's torsion problem by power series. *Int. J. Solids Structures* **11**, 321–328.

Nixon, M. W. (1987). Extension–twist coupling of composite circular tubes with application to tilt rotor blade design. *Proc. AIAA/ASME/ASCE/AHS 28th Structures, Structural Dynamics, and Mater. Conf.*, Monterey, California, Vol. 1, pp. 295–303. AIAA, New York.

Reissner, E. and Tsai, W. T. (1972). On the determination of the centers of twist and of shear for cylindrical shell beams. *ASME J. Appl. Mech.* **39**, 1098–1102.

Reyfield, L. W. (1985). Design analysis methodology for composite rotor blades. *Seventh DOD/NASA Conf. in Fibrous Composites in Structural Design*, Denver, Co., pp. 1–15.

Sokolnikoff, I. S. (1946). *Mathematical Theory of Elasticity*, 1st Edn. McGraw-Hill, New York.

Tolf, G. (1985). Saint-Venant bending of an orthotropic beam. *Compos. Struct.* **4**, 1–14.

Wörndle, R. (1982). Calculation of the cross-section properties and the shear stresses of composite rotor blades. *Vertica* **6**, 111–129.

Zienkiewicz, O. C. and Taylor, R. L. (1987). *The Finite Element Method*. McGraw-Hill, New York.

APPENDIX

The matrix $[\overline{F_{C_i}}]$ is defined as:

$$[\overline{F_{C_i}}] = \begin{bmatrix} -\frac{v_1}{EI_{yy}}x(z-L) & -\frac{v_1}{EI_{xx}}y(z-L) \\ -\frac{v_2}{EI_{yy}}x(z-L) & -\frac{v_2}{EI_{xx}}y(z-L) \\ -\frac{1}{2EI_{yy}}\{v_3x+v_4y-2(z-L)\}x-\frac{v_5}{2EA} & -\frac{1}{2EI_{xx}}\{v_3x+v_4y-2(z-L)\}y-\frac{v_4}{2EA} \\ -\frac{1}{EI_{yy}}\left\{\frac{v_6}{2}x+v_2y+v_4(z-L)\right\}x & \frac{1}{2EI_{xx}}\{(v_1x^2-v_2y^2)-2v_4y(z-L)\} \\ -\frac{1}{2EI_{yy}}\{(v_1x^2-v_2y^2)+2v_3x(z-L)\} & -\frac{1}{EI_{xx}}\left\{v_1x+\frac{v_6}{2}y+v_3(z-L)\right\}y \\ -\frac{v_6}{EI_{yy}}x(z-L) & -\frac{v_6}{EI_{xx}}y(z-L) \end{bmatrix}$$

$$\begin{bmatrix} 0 & 0 & 0 & 0 & 0 \\ 0 & 0 & 0 & 0 & 0 \\ \frac{1}{EA} & \frac{1}{EI_{xx}}y & -\frac{1}{EI_{yy}}x & \frac{v_5}{2EI_{xx}}y-\frac{v_4}{2EI_{yy}}x & 0 \\ 0 & 0 & 0 & 0 & x \\ 0 & 0 & 0 & 0 & -y \\ 0 & 0 & 0 & 0 & 0 \end{bmatrix} \quad \text{(A1)}$$

Integrating the matrix of (A1) over the beam length results in

$$\int_0^L [\overline{\overline{F_C}}]\,dz = L[\overline{\overline{F_C}}] \tag{A2}$$

where

$$[\overline{\overline{F_C}}] = \left[\begin{array}{cc|ccc} \frac{v_1 L}{2EI_{yy}}x & \frac{v_1 L}{2EI_{xx}}y & & & \\ \frac{v_2 L}{2EI_{yy}}x & \frac{v_2 L}{2EI_{xx}}y & & & \\ -\frac{1}{2EI_{yy}}\{v_5 x+v_4 y+L\}x-\frac{v_5}{2EA} & -\frac{1}{2EI_{xx}}\{v_5 x+v_4 y+L\}y-\frac{v_4}{2EA} & & & \\ -\frac{1}{2EI_{yy}}\{v_6 x+2v_2 y-v_4 L\}x & \frac{1}{2EI_{xx}}\{(v_1 x^2-v_2 y^2)+v_4 Ly\} & & & \\ -\frac{1}{2EI_{yy}}\{(v_1 x^2-v_2 y^2)-v_5 Lx\} & -\frac{1}{2EI_{xx}}\{2v_1 xy+v_6 y-v_5 L\}y & & & \\ \frac{v_6 L}{2EI_{yy}}x & \frac{v_6 L}{2EI_{xx}}y & & & \end{array}\right.$$

$$\left.\begin{array}{ccccc} 0 & 0 & 0 & 0 & 0 \\ 0 & 0 & 0 & 0 & 0 \\ \frac{1}{EA} & \frac{1}{EI_{xx}}y & -\frac{1}{EI_{yy}}x & \frac{v_5}{2EI_{xx}}y-\frac{v_4}{2EI_{yy}}x & 0 \\ 0 & 0 & 0 & 0 & x \\ 0 & 0 & 0 & 0 & -y \\ 0 & 0 & 0 & 0 & 0 \end{array}\right] \tag{A3}$$